Structural and elastic properties of perovskite HoMnO3 crystal structures from ab-initio calculations

Joël Martial Balkoulga, Antoine Béré, Sidiki Zongo, Viwanou Hounkpati, Moussa Sougoti, Sié Zacharie Kam, Jun Chen, Pierre Ruterana

Structural and elastic properties of perovskite $HoMnO_3$ crystal structures from ab-initio calculations

Joël Martial Balkoulga [1], Antoine Béré [1,*], Sidiki Zongo [1], Viwanou Hounkpati [2], Moussa Sougoti [1], Sié Zacharie Kam [1], Jun Chen [2], and Pierre Ruterana [3]

[1] *Laboratoire de physique et de chimie de l'environnement (LPCE), Université Joseph KI-ZERBO, Ouagadougou, Burkina Faso*
[2] *Centre de recherche sur les ions, les matériaux et la photonique (CIMAP), équipe PM2E, UMR6252 ENSICAEN-CNRS-UCN-CEA, IUT Grand Ouest Normandie, Pôle Universitaire d'Alençon, Campus de Damigny, 61250 Damigny, France*
[3] *Centre de recherche sur les ions, les matériaux et la photonique (CIMAP), équipe PM2E, UMR6252 ENSICAEN-CNRS-UCN-CEA, 6, Bd du Maréchal Juin, 14050 Caen, France*

Abstract

The structural and elastic properties of the oxide perovskite $HoMnO_3$ have been investigated by density-functional theory (DFT) implemented on the Quantum ESPRESSO code for the hexagonal, orthorhombic, rhombohedral and cubic crystal structures in the non-magnetic (NM), ferromagnetic (FM) and antiferromagnetic (AFM) configurations. The results show that all these compounds are thermodynamically stable, the hexagonal and the orthorhombic being the most stables in agreement with experimental results. The calculated bulk modulus, B, is about 168.5 ±1.0 GPa and 178.9 ±1.0 GPa for hexagonal structure in FM and configurations, respectively, and 188.7 ±0.6 GPa and 175.6 ±2.1GPa for orthorhombic structure in FM and AFM configurations, respectively. These values and those of the elastic constants C_{ij} in the present work are comparable to values recently obtained with DFT calculations and experimentally for other perovskites $RMnO_3$ (R=Eu, Gd, Tb and Dy). The calculated Poisson's ratio is about 0.19; 0.27; 0.23 and 0.3 for hexagonal, orthorhombic, rhombohedral and cubic structure, respectively. The calculated Pugh's ratio is about 1.30; 1.77-1.98; 1.54-1.60 and 2.11, respectively. These results show that the perovskite $HoMnO_3$ tends to be brittle in hexagonal

[*]Corresponding author: e-mail: antoine.bere@ujkz.bf

phase and ductile in cubic phase. In the orthorhombic or rhombohedral phase, it is near brittle-ductile boarder line.

Keywords: $HoMnO_3$; manganite crystal structures; manganite elastic constants; ab initio calculations; Quantum Espresso

I. INTRODUCTION

The manganese-based perovskite oxides of the $RMnO_3$ type recognized as multiferroic materials have attracted technological interest because they exhibit at least two ferroic orders, (anti)ferroelectricity, (anti)ferromagnetism and ferroelasticity, within a single phase offering the possibility of controlling the electrical polarization under a high magnetic field, or vice versa. They offer a wide range of potential applications such as high-density magnetic recording, magnetoresistive sensors and magnetic refrigeration [1], [2]. Under normal temperature and pressure conditions, the $RMnO_3$ perovskites can be structurally divided into three subgroups depending on the size of the rare earth element R. The former subgroup with small rare earth ionic radius (R = Sc, Y, Ho, Er, Tm, Yb and Lu), these perovskite crystallize in a hexagonal lattice named h-$RMnO_3$, mainly in the $P6_3cm$ space group. The second subgroup, with large rare earth ionic radius, crystallizes in an orthorhombic structure and is designated o-$RMnO_3$, mainly in the $Pnma$ space group. They are the compounds with R = La, Ce, Pr, Nd, Pm, Sm, Eu, Gd, Tb and Dy. The last subgroup (R = Ho, Y or Dy), with medium rare earth ionic radius, crystallizes either in hexagonal or orthorhombic structure depending on the synthesis conditions. Experimentally, it has been reported that the hexagonal phase of $RMnO_3$ can be transformed into orthorhombic phase at high temperature and pressure [3], [4].

To our knowledge, there is no systematic study including different crystal systems (cubic, hexagonal, orthorhombic, rhombohedral, etc.) of such perovskite $RMnO_3$ since some were synthesized under specific experimental conditions [5]. Indeed, previous theoretical works on $HoMnO_3$ reported the following crystal structures: hexagonal [6], [7]; orthorhombic [8], [9]; rhombohedral [10], and none of these works dealt with different crystal systems.

In this work, we have carried out a systematic DFT study based on Quantum ESPRESSO calculations of the structural and elastic properties of perovskite $HoMnO_3$ in its hexagonal (h-HMO), orthorhombic (o-HMO), rhombohedral (r-HMO) and cubic (c-HMO) structures. They

are in $P6_3cm$, $Pnma$, $R\bar{3}c$ and $Pm\bar{3}m$ space groups, respectively. It has to be noticed that there is a lack of experimental or theoretical data on elastic constants of this perovskite. Therefore, the objective of this study is to provide a better comparability of the obtained results.

II. THEORETICAL APPROACHES

2.1. Potential and structural properties

The Quantum Espresso code for first-principles calculations based on density functional theory (DFT) is employed as potential. This performs electronic structure calculations and materials (metals, insulators and semiconductors) modelling with high accuracy.

Quantum Espresso supports Norm-Conserving (NC), Ultrasoft (US), and Projector-Augmented Wave (PAW) pseudopotentials (PPs). It also supports exchange-correlation functions of the local density approximation (LDA), generalized gradient approximation (GGA), or more advanced type.

To run Quantum Espresso, some parameters are fixed. This includes, (i) the valence states describing the atomic cores; (ii) the pseudopotential describing the ion-electron interactions; (iii) the exchange-correlation functional; (iv) the convergence criterion on total energy for ionic minimization (etot_conv_thr); (v) the convergence criterion on forces for ionic minimization (forc_conv_thr); (vi) the k-point mesh to determine the first Brillouin zone; (vii) the kinetic energy cutoff for wavefunctions (ecutwfc) and (viii) the kinetic energy cutoff for charge density and potential (ecutrho). For this work, (i) the valence states are set to ($5s^2 6s^{1,5} 5p^6 6p^{0,5} 5d^1$), ($3s^2 3p^6 3d^5 4s^2$), and ($2s^2 2p^4$) for the Ho, Mn, and O atoms, respectively; (ii) the ion-electron interactions are described by the PAW method [11]; (iii) the exchange-correlation functional employed is that of Perdew-Burke-Ernzerhof parameterization of the generalized gradient approximation (PBE-GGA) [12]; (iv) the energy convergence criterion for electronic self-consistency is set to 10^{-6} u.a; (v) the atomic forces convergence criterion is set to 10^{-4} u.a; (vi)

the k-point mesh is set to 9 × 9 × 9; (vii) the kinetic energy cutoff for wavefunctions is set to 80 Ry and (viii) the kinetic energy cutoff for charge density and potential is set to 400 Ry. It has to be noticed that the values of these last three parameters are fixed after the energy convergence test calculations (Fig 1).

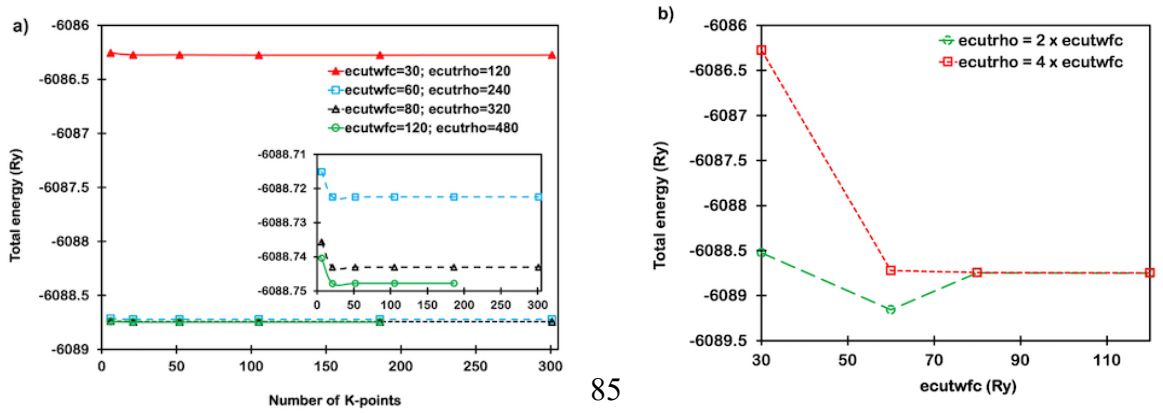

Fig1: Convergence test of total energy as a function of: a) k-points mesh; b) kinetic energy cutoff for wavefunctions (ecutwfc). In (a), the convergence is assumed to occur with 52-points that correspond to a 6 x 6 x 6 k-points grid and undependably of the ecutwfc value. In (b), the convergence is assumed to occur with ecutwfc=80 Ry and undependably of the ecutrho value.

Geometry optimizations are performed in the supercell method using the Broyden–Fletcher–Goldfarb–Shanno (BFGS) quasi-newton algorithm [13]; all atoms were allowed to relax and reach minimum energies when the atomic forces become less than 10^{-4} u.a. as previously mentioned.

When the lower energy relaxed structure is obtained, the formation energy is calculated to ensure that the system is thermodynamically stable. For compound materials such as $HoMnO_3$ in equilibrium with a reservoir of Ho, Mn and O atoms, the formation energy $E_{form}(D)$ of a given structure D is defined as [14]:

$$E_{form}(D) = E_{total}(D) - \mu_{H_O} \times n_{H_O} - \mu_{M_n} \times n_{M_n} - \mu_O \times n_O \quad (1)$$

where $E_{total}(D)$ is the total energy of the supercell while μ_{H_O} $\mu_{M_n}$and μ_O are the Ho, Mn and O chemical potentials, respectively. The values of these chemical potentials have been obtained from Quantum Espresso calculations in the C19_alpha_Sm prototype (space group = R-3m) for holmium (Ho), Mn(cI58) prototype (space group = I-43m) for manganese (Mn) and BaP3 prototype (space group = C2/m) for oxygen (O). The quantities n_{H_O} , n_{M_n} , and n_O correspond to the numbers of Ho, Mn and O atoms, respectively. The numbers of atoms per unit cell and its repartition per atomic specie, $n_{tot}(n_{H_o}, n_{M_n}, n_O)$ are: $30(6,6,18)$ for h-HMO or r-HMO; $20(4,4,12)$ for o-HMO and $5(1,1,3)$ for c-HMO.

The most stable structure is obtained by comparing the energy of a given structure (i) to a reference structure (ref) by evaluating the relative energy $\Delta E(i)$ defined as:

$$\Delta E(i) = E_{form}(i) - E_{form}(ref) \quad (2)$$

where $E_{form}(i)$ and $E_{form}(ref)$ are the formation energies of the structure (i) and the reference structure, respectively. In present calculations, the reference structure is set to the h-HMO structure in the FM configuration.

2.2. Elastic constant calculations

The elastic properties of a crystal can be characterized by independent elastic constants, namely C_{ij}. The total number of independent components of the elastic constant tensor depends on the symmetry of the crystal. There are two approaches for calculating elastic constants: the energy-strain $(E-\varepsilon)$ method and the stress-strain $(\sigma-\varepsilon)$ method. For more details on these methods, see the publications of [15], [16], [17]. From these two methods, the energy–strain is a more common-place for calculations using DFT approach. In this method, the energy of the crystal is calculated for different values of the strain ε. Then, its evolution curve is fitted as a function of ε by a polynomial and the value of the second derivative at ε =0 related to those of C_{ij} is deduced. It should be noted that there are two parameters to be chosen for this method:

the polynomial degree and the ε region on which the adjustment is performed. In the present work, the study focuses on ε region ranging from -0.06 to 0.06 with a step of 0.02. This gives rise to seven self-consistent energy calculations for a given C_{ij} calculation or their combination. The fitting of polynomial of order 3 and 4 was performed, allowing the determination of average values and deviations.

It is well known that the elastic computation via the energy–strain relationship can lead to erroneous results at non-zero pressure. Then, when the elastic constants are calculated, the elastic stabilities of the four investigated structures are tested according to the stability criteria presented in Table 1.

Table 1: Elastic stability of crystal systems

Crystal systems	Point groups	Space groups	Born stability criteria [18]
Cubic	$m\bar{3}m$	$Pm\bar{3}m$	$C_{11} - C_{12} > 0; C_{11} + 2C_{12} > 0; C_{44} > 0$
Hexagonal	6mm	$P6_3cm$	$\begin{cases} C_{11} > \lvert C_{12}\rvert;\ 2C_{13}^2 < C_{33}(C_{11} + C_{12}) \\ C_{44} > 0;\ C_{66} > 0 \end{cases}$
Orthorhombic	Mmm	Pnma	$\begin{cases} C_{11} > 0;\ C_{11}C_{22} > C_{12}^2; \\ C_{11}C_{22}C_{33} + 2C_{12}C_{13}C_{23} - C_{11}C_{23}^2 - C_{22}C_{13}^2 - C_{33}C_{12}^2 > 0 \\ C_{44} > 0;\ C_{55} > 0; C_{66} > 0 \end{cases}$
Rhombohedral	3m	$R\bar{3}c$	$\begin{cases} C_{11} > \lvert C_{12}\rvert;\ C_{44} > 0 \\ C_{13}^2 < \frac{1}{2}C_{33}(C_{11}+C_{12}) \\ C_{14}^2 < \frac{1}{2}C_{44}(C_{11}-C_{12}) = C_{44}C_{66} \end{cases}$

To predict the plastic behavior of materials, the most widely used criteria are the Poisson's ratio, $\nu = \frac{3B-2G}{2(3B+G)}$, and the Pugh's ratio, $\frac{B}{G}$, where B is the bulk modulus and G is the shear modulus. Each of these ratios is related to the competition between two mechanical processes, fracture and plasticity. For a given material, if plasticity (fracture) is easier, then it will tend to be ductile (brittle). The critical value is 0.26 and 1.75 for the Poisson's ratio and the Pugh's

ratio, respectively [19][20]. The material is considered ductile (brittle) for a value of the Poisson's ratio or Pugh's ratio greater (smaller) than the corresponding critical value. In the present work, the Poisson's ratio and the Pugh's ratio are calculated according to Voigt-Reuss-Hill approximations [21].

III RESULTS AND DISCUSSION

3.1 Structural and magnetic properties

The structural properties which have been investigated are the lattice parameters, the formation energies and the relative stabilities of the different structures. The magnetic behaviour is determined by taking into account the non-magnetic (NM), ferromagnetic (FM) and the anti-ferromagnetic (AFM) spin configurations of the studied crystal systems (h-HMO, o-HMO, r-HMO and c-HMO). To this end, geometrical optimization calculations were first performed as described previously. The energy versus volume curves for different crystal phases in FM and AFM configurations of the $HoMnO_3$ structure is presented in figure 2. It comes that the lowest energy configuration for $HoMnO_3$ is the hexagonal structure (Ishibashi et al.). The least stable phase is the cubic structure. The minimum energy of the orthorhombic structure is closer to that of the hexagonal structure than the rhombohedral structure. The FM and AFM configurations of the hexagonal, orthorhombic or rhombohedral structure have almost identical evolution curves.

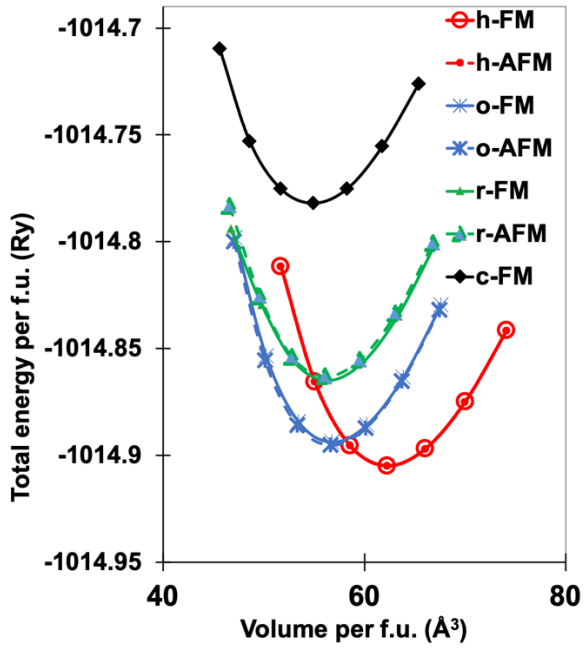

Fig2: Energy versus volume for $HoMnO_3$ different crystal structures in FM and FM configurations. The number of atoms in the unit cell is 30, 20, 30 and 5 for h-HMO, o-HMO, r-HMO and c-HMO, respectively. This gives rise to the unit formula (f.u.) per unit cell of 6, 4, 6 and 1 for h-HMO, o-HMO, r-HMO and c-HMO, respectively. On the legend, h-FM refers to h-HMO in FM configuration.

3.1.1. Lattice parameters

The lattice parameters in the FM, AFM and NM configurations of h-HMO, o-HMO, r-HMO and c-HMO relaxed atomic structures (figures 3-6) are presented in Table 2 in comparison with reported theoretical and experimental data. The h-HMO lattice parameters values are in good agreement with the recent experimental results of Ishibashi et al. [4]. Also, the o-HMO lattice parameters are in agreement with the experimental results of Alonso et al. [22] than theoretical results reported in [23], [8]. In the case of r-HMO and c-HMO lattice parameters, in absence of experimental data, our results compare well with those of theoretical reported in [24].

The good agreement of the obtained values with those of experimental demonstrates the accuracy of the quantum expresso calculations.

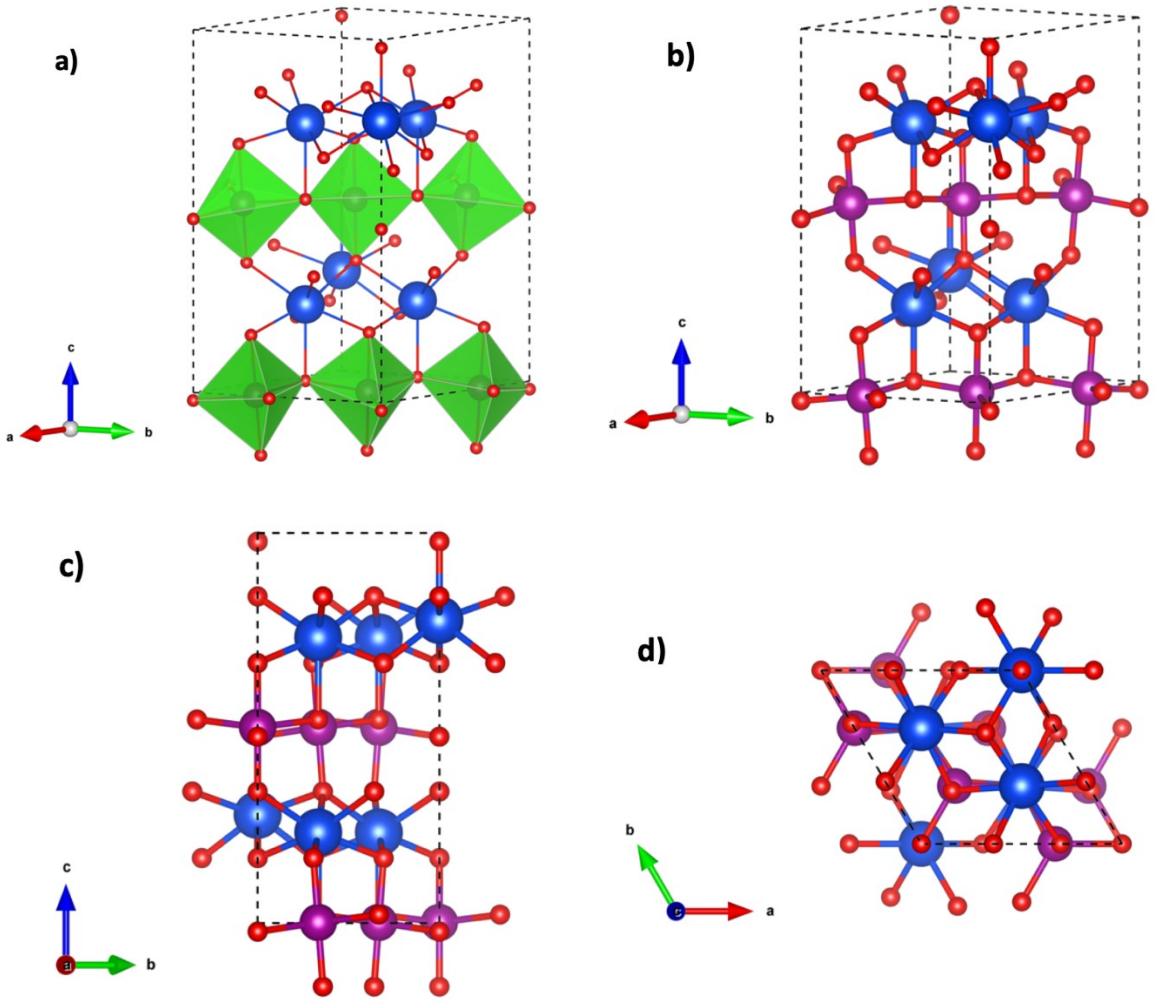

176

177 *Fig3: Relaxed atomic structure of $HoMnO_3$ hexagonal crystal phase in FM configuration. a)*
178 *structure along* [001]; (b) the real cell; (c) in a-direction; and in c-direction. The blue, purple
179 and red balls correspond to Ho, Mn and O atoms, respectively. The MnO_5 trigonal bipyramid
180 is represented in green. The unit cell is shown by dashed lines.

181

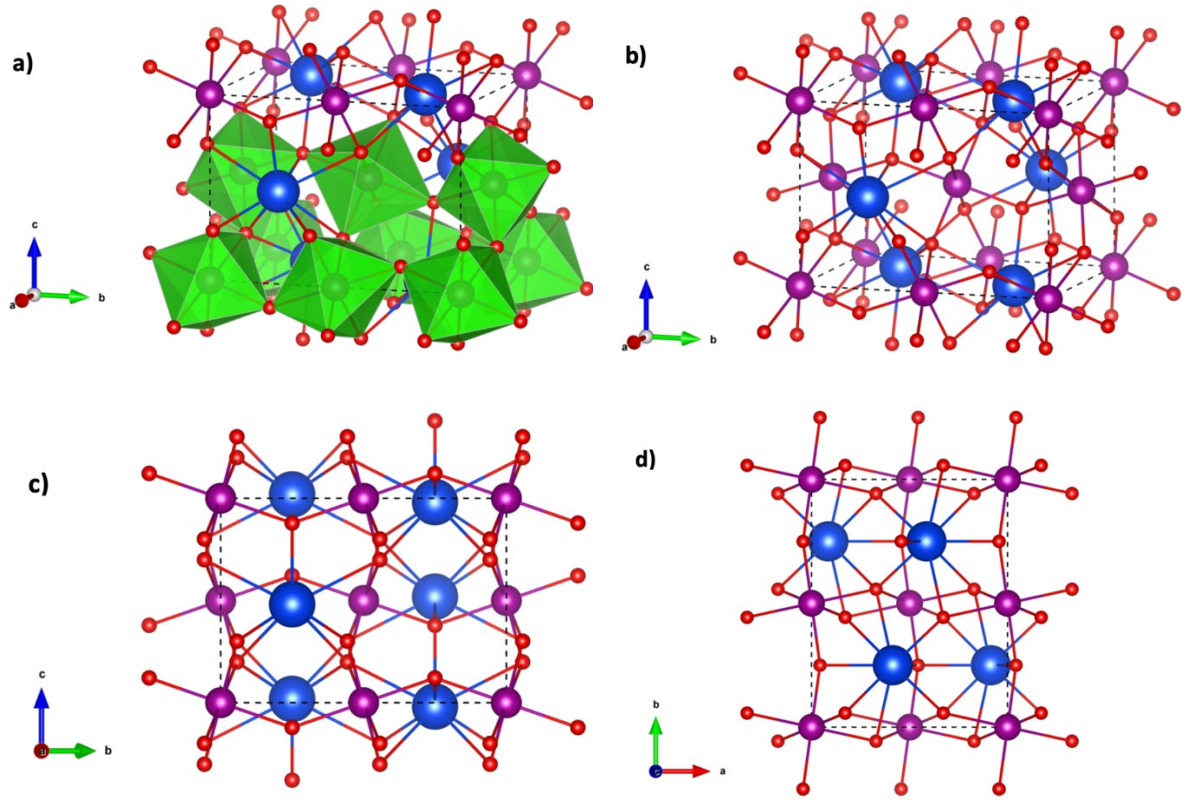

Fig4: Relaxed atomic structure of $HoMnO_3$ orthorhombic crystal phase in FM configuration. a) structure along [001]; (b) the real cell; (c) in a-direction; and in c-direction. The blue, purple and red balls correspond to Ho, Mn and O atoms, respectively. The MnO_6 octahedra are represented in green. The unit cell is shown by dashed lines.

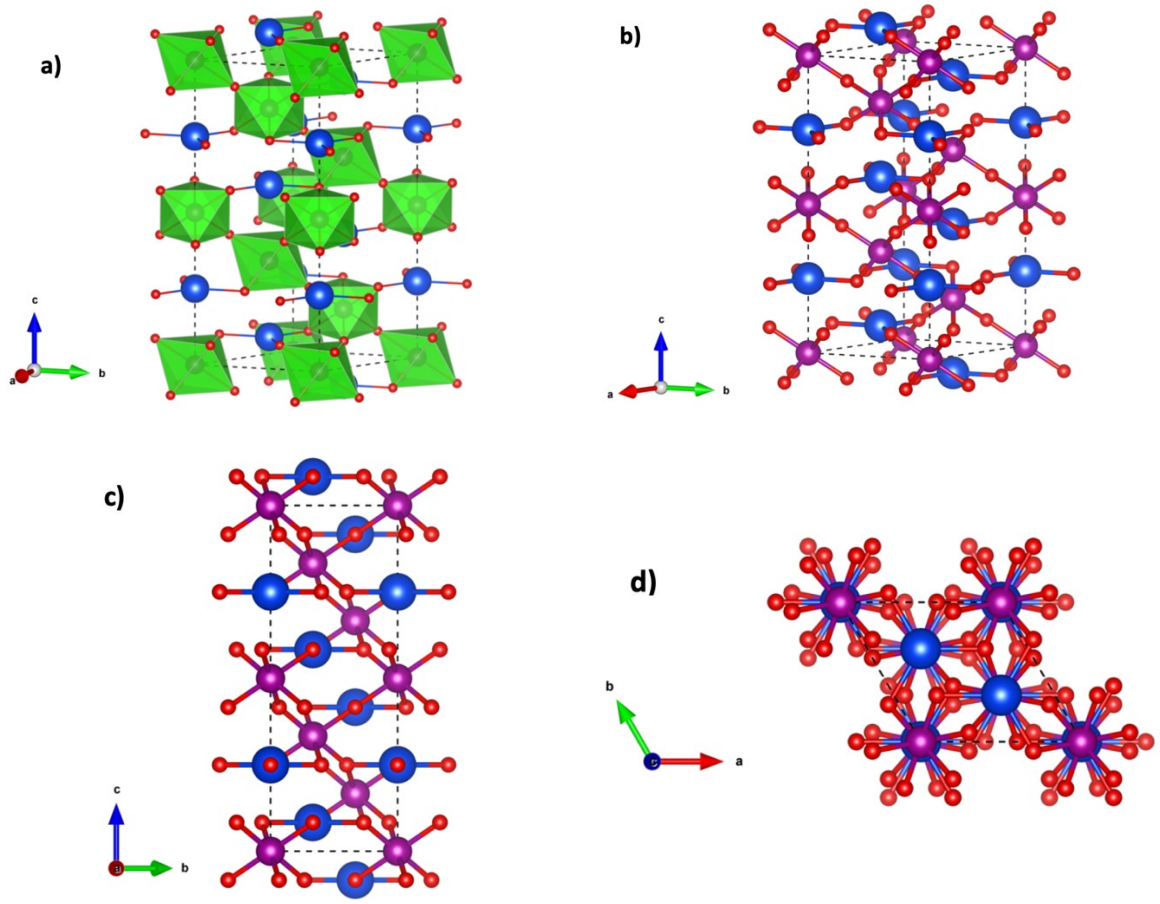

186

187 *Fig5: Relaxed atomic structure of $HoMnO_3$ rhombohedral crystal phase in FM configuration.*
188 *a) structure along* [001]; (b) the real cell; (c) in a-direction; and in c-direction. The blue, purple
189 and red balls correspond to Ho, Mn and O atoms, respectively. The MnO_6 octahedra are
190 represented in green. The unit cell is shown by dashed lines.

191

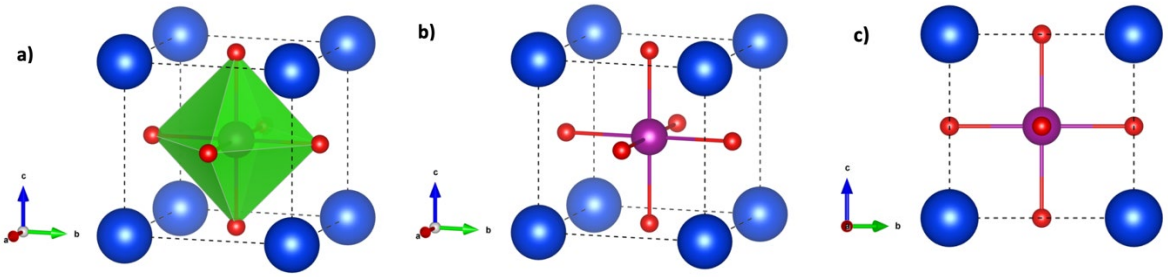

Fig6: Relaxed atomic structure of $HoMnO_3$ cubic crystal phase in FM configuration. a) structure along [001]; (b) the real cell; (c) in a-direction; and in c-direction. The blue, purple and red balls correspond to Ho, Mn and O atoms, respectively. The MnO_6 octahedra is represented in green. The unit cell is shown by dashed lines.

198 *Table 2: Lattice parameters, a, b and c, in angstrom (**Å**), equilibrium unit cell volume, V, in*
199 ***Å**³, formation energy, E_{form}, in electron-volt per atom (**eV**/atom), and relative energy, ΔE, in*
200 *millielectron-volt per atom (m**eV**/atom) obtained with PBE-GGA-APW pseudopotentials DFT*
201 *calculations for $HoMnO_3$ crystal structures in non-magnetic (NM), ferromagnetic (FM) and*
202 *antiferromagnetic (AFM) configurations.*

Structure	a (Å)	b (Å)	c (Å)	V (Å³)	E_{form} (eV/atom)	ΔE (meV/atom)	Ref.
h-HMO							
NM	6.0562	6.0562	11.3160	359.68	-2.435	311	P.W.[1]
	NI[2]	NI	NI	NI	NI	394 [3]	[7]
FM	6.1463	6.1463	11.4181	373.51	-2.746	0	P.W.
	6.1300	6.1300	11.4340	372.06	-2.965	0	[24]
	6.1450	6.1450	11.4190	373.62	NI	NI	[4]
	6.1382	6.1382	11.4118	372.61	NI	NI	[25]
	6.1413	6.1314	11.4122	372.75	NI	NI	[26]
	6.1477	6.1477	11.4898	376.07	NI	0	[7]
AFM	6.1412	6.1412	11.4147	373.42	-2.746	0	P.W.
	6.1522	6.1522	11.5125	377.36	NI	-24 [3]	[7]
o-HMO							
NM	5.5440	7.3756	5.1065	208.81	-2.515	230	P.W.
FM	5.8461	7.3742	5.2681	227.11	-2.716	30	P.W.
	5.7100	7.4640	5.2570	224.06	-2.874	31	[24]
	5.8354	7.3606	5.2572	225.81			[22]
	5.7790	7.4410	5.2130	224.20			[23]
AFM	5.9039	7.3292	5.2387	226.68	-2.720	26	P.W.
	5.7500	7.2530	5.1800	216.01		679 [4]	[8]
r-HMO							
NM	5.3910	5.3910	12.4293	312.84	-2,450	296	P.W.
	NI	NI	NI	NI	NI	631	[10]
FM	5.4894	5.4894	12.9427	337.76	-2.637	109	P.W.
	5.4700	5.4700	12.8230	332.27	-2.874	122	[24]
	5.5960	5.5960	13.1210	355.84	NI	NI	[10]
AFM	5.4771	5.4771	12.9567	336.61	-2.632	114	P.W.
	NI	NI	NI	NI	NI	28; 112	[10]
c-HMO							
NM	3.7344	3.7344	3.7344	52.08	-2.240	506	P.W.
FM	3.8042	3.8042	3.8042	54.92	-2.411	334	P.W.
	3.8250	3.8250	3.8250	55.97	-2.639	357	[24]

[1] Present work
[2] Not indicated in the publication
[3] According to [7], the h-HMO relative energies with respect to the AFM configuration are 0.72 and 12.53 eV in FM and NM configurations, respectively. When taking the FM configuration as reference and considering that its supercell contains 30 atoms, we deduce that the h-HMO relative energies with respect to the FM configuration are -24 and 394 meV/atom in the AFM and NM configurations, respectively.
[4] According to [8], the o-HMO total energies are -112105.73656421 and -112104.738371 Ry in FM and AFM configurations, respectively. When considering that its supercell contains 20 atoms, we deduce that the o-HMO relative energy with respect to the FM configuration is 679 meV/atom in the AFM configuration.

Table 3 shows a comparison between the Mn-O and Ho-O interatomic distances. The notation for Ho (Ho1 and Ho2), O (O1, O2, O3 and O4) and Mn is similar to those adopted in Refs.[4]. As results, we obtain that the calculated interatomic distances in this present work are in good agreement with reported experimental [4] and theoretical [8] works. In general, the Ho-O interatomic distances are larger than the Mn-O distances, mainly the distances along of the c-axis (Ho-O3 and Ho-O4). The results show small changes for interatomic distances and tilting angles of the MnO_5 polyhedron in the FM and AFM configurations. Experimental analysis of the chemical bonding is needed in order to explain these constatations.

Table 3: Interatomic distance (Mn-O and Ho-O) and angles (O-Mn-O) of the MnO_n polyhedron for $HoMnO_3$ relaxed *atomic structures in ferromagnetic (FM) and antiferromagnetic (AFM) configurations.*

Structural parameter	**Experimental [4]**	**Present work**		**Previously calculated [8]**
		FM	**AFM**	
Hexagonal phase				
Ho1-O1/Å	2.308 x 3	2.312 x 3	2.312 x 3	
Ho1-O2/Å	2.324 x 3	2.270 x 3	2.270 x 3	
Ho1-O3/Å	2.380 x 1	2.292 x 1	2.292 x 3	
Ho2-O1/Å	2.244 x 3	2.308 x 3	2.308 x 3	
Ho2-O2/Å	2.359 x 3	2.263 x 3	2.263 x 3	
Ho2-O4/Å	2.410 x 1	2.405 x 1	2.405 x 1	
Mn-O1/Å	1.865 x 1	1.885 x 1	1.885 x 1	
Mn-O2/Å	1.960 x 1	1.890 x 1	1.889 x 1	
Mn-O3/Å	1.993 x 1	2.068 x 1	2.080 x 1	
Mn-O4/Å	2.092 x2	2.062 x 2	2.056 x 2	
01-Mn-O2/°		179.835	179.47	
03-Mn-04/°		120.392	119.18	
Orthorhombic phase				
Ho-O/Å		2.225 x 1	2.226 x 1	2.313
		2.279 x 2	2.270 x 2	2.266
		2.292 x 1	2.293 x 1	
		2.501 x 2	2.509 x 2	
		2.586 x 2	2.560 x 2	
Mn-O/Å		1.922 x 4	1.904 x 2	1.898
			1.956 x 2	1.984
		2.228 x 2	2.269 x 2	
Rhombohedral phase				

Structural parameter	Experimental [4]	Present work		Previously calculated [8]
		FM	AFM	
Ho-O/Å		2.195 x 3	2.213 x 3	
Mn-O/Å		1.994 x 6	1.964 x 3	
			2.010 x 3	
Cubic phase				
Ho-O/Å		2.890 x 6		
Mn-O/Å		1.902 x 6		

214

215 *3.1.2. Magnetic behavior*

216 The formation energies E_{form} in the FM, AFM and NM configurations of h-HMO, o-HMO,
217 r-HMO and c-HMO crystal structures are presented in Table 2. The obtained values compare
218 well with those reported in [24]. The negative sign of the formation energies means that all
219 these crystal structures in different spin configurations are thermodynamically stable.

220 The magnetic behavior is discussed by evaluating the stability of corresponding
221 configuration compared with FM state. It appears from the relative energies ΔE deduced from
222 formation energies (Table 2) that whatever the considered crystal structure, its magnetic
223 configuration (FM or AFM) is the most stable whereas its non-magnetic configuration (NM)
224 is the most unstable. Also, with respect to the orders of magnitude of the absolute values of the
225 relative energies, it appears unambiguous that the h-HMO structure is energetically more
226 favorable than the o-HMO, r-HMO and c-HMO structures. Our results also show that the FM
227 configuration is more energetically favorable than the AFM configuration for all crystal
228 structures, in agreement Hamioud et al. [8] for the case of o-HMO, using Wien2k code.
229 However, this is in opposite with the result reported by Chadli et al. [7] for the case of h-HMO
230 which calculations are done with the VASP code.

231 ***3.1. Elastic properties***

232 The calculated elastic constants and bulk modulus are presented in Table 4. To our
233 knowledge, there is no experimental data on these parameters for $HoMnO_3$ crystal structures.
234 The existing results of the perovskite HoMnO3 based on DFT calculations concern its bulk

modulus [7], [8], but not for the elastic constants C_{ij}. The present work is the first evaluation of the elastic constants of the perovskite $HoMnO_3$ based on ab-initio calculations. Consequently, the calculated values could not be compared with experimental data. Also, the theoretical data on perovskite similar to $RMnO_3$ type [23], [27], [28], [29] are given in Table 4 to serve for comparison.

3.1.1. Bulk modulus

The h-HMO bulk modulus is 168.5 ±1.0 and 178.9 ±1.0 GPa for FM and AFM configurations, respectively. These values agree with those of 162.23 GPa and 169.34 GPa reported by Chadli et al. [7]. For the o-HMO structure, the calculated bulk modulus is 188.7 ±0.6 GPa and 175.6 ±2.1 GPa for the FM and AFM configurations, respectively. These values are smaller than the value of 201.64 GPa reported by Hamioud et al. [8]. However, they are in agreement with experimental data reported by Muthu et al. [27] for others perovskites RMnO3 that include $EuMnO_3$ (185±6 GPa), $GdMnO_3$ (190±16 GPa), $TbMnO_3$ (188±9 GPa) and $DyMnO_3$ (192±8 GPa) in orthorhombic phase. From these four perovskites, the $DyMnO_3$ is classified in the same subgroup as the $HoMnO_3$. The bulk modulus value of $HoMnO_3$ is smaller than that of $DyMnO_3$. This result leads to the conclusion that $HoMnO_3$ is more flexible than $DyMnO_3$.

3.1.2. Elastic constants

According to Tables 4 and 5, the elastic constants of the present work are 1.6 to 2.3 times higher than those given by Shell model calculations reported for the o-HMO structure [23] and for three other perovskites of $RMnO_3$ type [28]. However, the calculated elastic constants are in the same order with those of DFT calculations and measured elastic constants as reported by Hemme et al. [29]. We conclude that a discrepancy is clear with results obtained from shell-model potential calculations.

Also, the calculated elastic constants satisfy the necessary and sufficient conditions for elastic stability given in Table 1 for each of the four investigated structures.

3.1.3. Mechanical behavior

Table 6 displays the calculated bulk modulus (B), shear modulus, (G) Young's modulus **E**, Poisson's ratio (ν) and Pugh's ratio (B/G) for $HoMnO_3$ different crystal structures in FM and AFM configurations according to Voigt-Reuss-Hill (VRH) approximations [21]. It is interesting to note that the bulk modulus values are comparable with those obtained from the strain-energy method (Table 4). For the FM (AFM) configuration, the deviation is about 1.06% (1.08%) for h-HMO, 0.21% (2.97%) for o-HMO, 0.85% (1.91%) for r-HMO and -0.73% for c-HMO.

The calculated values of ν and B/G indicate that $HoMnO_3$ is brittle in the hexagonal phase (ν=0.19 and B/G=1.3) and ductile in the cubic phase (ν=0.30 and B/G=2.11). In the orthorhombic phase (ν=0.26-0.28 and B/G=1.77-1.98) or rhombohedral phase (ν=0.23-0.24 and B/G=1.54-1.60), it is difficult to conclude with certainty whether the material is ductile or brittle. They are near brittle-ductile boarder line. According to [30], the calculated values of ν predict that $HoMnO_3$ tends to be ionic material (ν~0.1) in the hexagonal phase, metallic material (ν~0.33) in the cubic phase and covalent material (ν~0.25) in the orthorhombic or rhombohedral phase.

The calculated value of Young's modulus of the hexagonal phase (E=305 GPa) is higher than that of 219.2 ± 10.6 GPa reported experimentally [31].

The bulk modulus is an indicator of compound's resistance to the volume change. Usually, the bulk modulus increases when the cell volume decrease. Our calculated bulk moduli are about 154, 167, 172 and 181 GPa for the cubic, hexagonal, rhombohedral and orthorhombic phases, respectively. The cell volumes are 10.98, 12.45, 11.26 and 11.36 $Å^3$/atom, respectively.

283 It appears that the above general trend doesn't correlate for the hexagonal phase which should
284 be expected to have the greater value of bulk modulus in correlation with its cell volume. We
285 conclude that an anomalous decreased as compared to the theoretical predictions is then
286 observed.

287

Table 4 : Elastic constants (C_{ij}) and bulk modulus (B) in GPa obtained with PBE-GGA-APW pseudopotentials DFT calculations for $HoMnO_3$ crystal structures in ferromagnetic (FM) and antiferromagnetic (AFM) configurations

Structure	Elastic constants								Bulk modulus	Ref.
	C_{11}	C_{22}	C_{33}	C_{12}	C_{13}	C_{23}	C_{44}	C_{66}	B	
h-HMO										
FM	293.4±1.3	293.4±1.3	385.3 ±5.6	69.1 ±0.4	103.0 ±4.7	103.0 ±4.7	175.5 ±0.2	83.3 ±0.3	168.5 ±1.0	P.W.[5]
AFM	293.1 ±1.3	293.1 ±1.3	384.7 ±5.9	69.3 ±4.1	103.0 ±7.4	103.0 ±7.4	175.8 ±0.2	83.4 ±0.4	168.4 ±1.0	P.W.
o-HMO										
FM	278.4 ±1.7 178	291.5 ±3.4 143	349.3 ±2.1 201	144.7 ±2.8	123.3 ±4.1	121.3 ±5.4	98.7 ±1.0 43	108.2 ±0.6	188.7 ±0.6	P.W. [23]
AFM	274.0 ±3.5	303.8 ±3.8	353.1 ±3.0	135.0 ±5.1	115.5 ±4.8	99.9 ±2.3	107.3 ±0.6	110.2 ±0.5	186.4 ±2.3	P.W.
r-HMO										
FM	364.6 ±0.7	364.6 ±0.7	221.1 ±2.5	146.2 ±4.1	93.9 ±3.3	93.9 ±3.3	148.5 ±1.8	80.5 ±0.9	173.9 ±14.5	P.W.
AFM	353.3 ±3.3	353.3 ±3.3	232.1 ±0.6	152.9 ±2.0	98.0 ±2.0	98.0 ±2.0	131.5 ±6.9	75.1 ±1.5	178.9 ±9.3	P.W.
c-HMO										
FM	305.5 ±8.4	305.5 ±8.4	305.5 ±8.4	79.5 ±9.2	79.5 ±9.2	79.5 ±9.2	54.7 ±2.3	54.7 ±2.3	153.7 ±3.7	P.W.

[5] Present work

Table 5 :Elastic constants in GPa of perovskite RMnO3 (R=Tb, Dy, Sm, Eu and Gd)

Structure	Elastic constants							Method	Ref.
	C_{11}	C_{22}	C_{33}	C_{12}	C_{13}	C_{23}	C_{44}		
o-$TbMnO_3$	185; 209; 174; 249	255; 277; 268; 301	239; 257; 265; 275	131; 147; 141; 173	93; 117; 109; 118	110; 128; 121; 144	87; 91; 43; 76	DFT	[29]
		202±20	181±2			103±6	71±5	Expt.[6]	
	227	349	274	141	109	103	71	Expt.	
	170	150	197				48	Shell model	[23]
o-$DyMn0_3$	170	151	196				48	Shell model	[23]
o-$SmMnO_3$	157	149	190				52		[28]
o-$EuMnO_3$	165	154	194				50		
o-$GdMnO_3$	166	143	198				45		

[6] Experimental

Table 6 : Calculated values of Bulk modulus (B), shear modulus G (GPa), Young's modulus E (GPa), Poisson'ratio (ν) and Pugh's ratio (B/G) for HoMnO3 different crystal structures in FM and AFM configurations according to Voigt-Reuss-Hill (VRH) approximations [21]

	B_V	B_R	G_V	G_R	B_{VRH}	G_{VRH}	E	ν	B/G
h-HMO									
FM	169.14	164.27	133.33	122.29	166.71	127.81	305.39	0.19	1.30
AFM	169.06	164.21	133.37	122.29	166.63	127.83	305.40	0.19	1.30
o-HMO									
FM	188.64	187.97	96.45	93.97	188.31	95.21	244.43	0.28	1.98
AFM	181.30	180.76	103.66	100.99	181.03	102.33	258.31	0.26	1.77
r-HMO									
FM	179.81	165.06	116.59	107.83	172.43	112.21	276.63	0.23	1.54
AFM	181.83	169.92	106.93	100.78	175.88	103.86	260.33	0.25	1.69
c-HMO									
FM	154.83	154.83	78.02	68.92	154.83	73.47	190.31	0.30	2.11

IV CONCLUSION

In summary, the structural and elastic properties of $HoMnO_3$ crystal systems have been investigated using accurate ab-initio calculations. The calculated formation energy shows that the rhombohedral or cubic structure should exist; however, the hexagonal and orthorhombic phases are energetically more favorable and the hexagonal crystal system is the most stable. The elastic properties have been for the first time, systematically studied. Due to the lack of experimental data, our results are predictive and are comparable to recent results on other perovskite $RMnO_3$ systems based on DFT calculations. The discrepancy is clear with results obtained from shell-model potential calculations. From this work, it may be concluded that such quantum espresso calculations are suitable and appropriate for the description of perovskite $RMnO_3$, mainly the subgroup exhibiting hexagonal or orthorhombic crystal structure (R=Dy or Ho.)

Acknowledgements: The computations were performed at “CRIANN” (http://www.crihan.fr).

References:

1. Lottermoser T, Meier D (2020) A short history of multiferroics. Physical Sciences Reviews 6:. https://doi.org/10.1515/psr-2020-0032
2. Kumar M, Shankar S, Kumar A, et al (2020) Progress in multiferroic and magnetoelectric materials: applications, opportunities and challenges. Journal of Materials Science: Materials in Electronics 31:19487–19510. https://doi.org/10.1007/s10854-020-04574-2
3. Wu Y, Xie Q, Li M, et al (2019) Structural and ferroelectric properties of orthogonal crystalline in Fe-doped HoMnO3 synthesized at normal pressure. Journal of Materials Science: Materials in Electronics 30:7629–7636. https://doi.org/10.1007/s10854-019-01078-6
4. Ishibashi H, Cubillas F, Uchihashi K, et al (2022) Phase diagram and crystal structure of Ti-doped HoMnO3 by high-resolution synchrotron powder diffraction. Journal of Solid State Chemistry 312:123273. https://doi.org/10.1016/j.jssc.2022.123273
5. Wood VE, Austin AE, Collings EW, Brog KC (1973) Magnetic properties of heavy-rare-earth orthomanganites. Journal of Physics and Chemistry of Solids 34:859–868. https://doi.org/10.1016/S0022-3697(73)80088-5
6. Brito DMS, Lima AF, Lalic MV (2023) Photoferroic prospective of multiferroic HoMnO3 compound, evaluated on the base of the DFT study of its magnetic, electronic, and optical properties. Journal of Physics and Chemistry of Solids 177:111301. https://doi.org/10.1016/j.jpcs.2023.111301
7. Chadli A, Lagoun B, Aissani L, et al (2022) Ab initio study including spin–orbit coupling of the electronic band structure and magnetic properties of h-HoMnO3. Indian Journal of Physics 96:1731–1739. https://doi.org/10.1007/s12648-021-02129-7
8. Hamioud F, Tariq S, Batool A, Mubarak AA (2020) Theoretical investigation on orthorhombic XMnO3 (X = Nd, Dy and Ho) perovskite manganates using DFT. Chemical Physics Letters 760:138005. https://doi.org/10.1016/j.cplett.2020.138005
9. Stroppa A, Picozzi S (2009) Hybrid functional study of proper and improper multiferroics. Physical chemistry chemical physics : PCCP 12 20:5405–16. https://doi.org/10.1039/b927508h
10. Li T, Khenata R, Khachai H, Wang X (2019) DFT-Based Study on Electronic, Magnetic and Thermodynamic Properties of HoMnO3: A Half-Metallic Material with Nearly Linear Band Crosses. SPIN 09:1940009. https://doi.org/10.1142/S2010324719500176
11. Kresse G, Joubert DP (1999) From ultrasoft pseudopotentials to the projector augmented-wave method. Physical Review B 59:1758–1775. https://doi.org/10.1103/PhysRevB.59.1758
12. Perdew, Burke, Ernzerhof (1996) Generalized Gradient Approximation Made Simple. Physical review letters 77 18:3865–3868. https://doi.org/10.1103/PhysRevLett.77.3865
13. Fletcher R (1987) Practical methods of optimization; (2nd ed.). Wiley
14. Béré A, Ruterana P, Nouet G, et al (2005) Density-functional tight-binding calculations of electronic states associated with grain boundaries in GaN. Phys Rev B 71:125211. https://doi.org/10.1103/PhysRevB.71.125211

15. Wallace DC (1972) Thermodynamics of Crystals
16. Perger WF, Criswell J, Civalleri B, Dovesi R (2009) Ab-initio calculation of elastic constants of crystalline systems with the CRYSTAL code. Comput Phys Commun 180:1753–1759. https://doi.org/10.1016/j.cpc.2009.04.022
17. Mehta S (2020) Calculation of elastic constants at high pressure from first-principles. AIP Conference Proceedings 2272:070032. https://doi.org/10.1063/12.0001097
18. Mouhat F, Coudert F-X (2014) Necessary and Sufficient Elastic Stability Conditions in Various Crystal Systems. Physical Review B 90:224104. https://doi.org/10.1103/PhysRevB.90.224104
19. Hamioud F, Mubarak AA (2018) Structural, elastic and optoelectronic properties of the hydrogen based perovskite compounds: Ab-initio study. Chinese Journal of Physics 56:1–9. https://doi.org/10.1016/j.cjph.2017.11.021
20. Tariq S, Alsalmi O, Alrashdi AO, et al (2021) Investigating the influence of pressure on SrFeO3 and SrMnO3 ferromagnets for high-pressure spintronic devices: a comparative DFT overview. Applied Physics A 127:902. https://doi.org/10.1007/s00339-021-05052-0
21. Wu Z, Zhao E, Xiang H, et al (2007) Crystal structures and elastic properties of superhard \mathrmIr\mathrmN_2 and \mathrmIr\mathrmN_3 from first principles. Phys Rev B 76:054115. https://doi.org/10.1103/PhysRevB.76.054115
22. Alonso JA, Martínez-Lope MJ, Casais MT, Fernández-Díaz MT (2000) Evolution of the Jahn−Teller Distortion of MnO6 Octahedra in RMnO3 Perovskites (R = Pr, Nd, Dy, Tb, Ho, Er, Y): A Neutron Diffraction Study. Inorg Chem 39:917–923. https://doi.org/10.1021/ic990921e
23. Choithrani R, Rao MN, Chaplot SL, et al (2011) Structural and phonon dynamical properties of perovskite manganites: (Tb, Dy, Ho)MnO3. Journal of Magnetism and Magnetic Materials 323:1627–1635. https://doi.org/10.1016/j.jmmm.2011.01.026
24. Kirklin S, Saal JE, Meredig B, et al (2015) The Open Quantum Materials Database (OQMD): assessing the accuracy of DFT formation energies. npj Computational Materials 1:15010. https://doi.org/10.1038/npjcompumats.2015.10
25. Gao P, Chen Z, Tyson TA, et al (2011) High-pressure structural stability of multiferroic hexagonal R\mathrmMnO_3 (R=\mathrmY, Ho, Lu). Phys Rev B 83:224113. https://doi.org/10.1103/PhysRevB.83.224113
26. Muñoz A, Casais MT, Alonso JA, et al (2001) Complex Magnetism and Magnetic Structures of the Metastable HoMnO3 Perovskite. Inorg Chem 40:1020–1028. https://doi.org/10.1021/ic0011009
27. Muthu DVS, Midgley AE, Scott PR, et al (2012) High - pressure synchrotron x-ray diffraction study of RMnO3 (R = Eu, Gd, Tb and Dy) upto 50 GPa. Journal of Physics: Conference Series 377:012025. https://doi.org/10.1088/1742-6596/377/1/012025
28. Choithrani R, Rao MN, Chaplot SL, et al (2009) Lattice dynamics of manganites RMnO3 (R =Sm, Eu or Gd): instabilities and coexistence of orthorhombic and hexagonal phases. New Journal of Physics 11:073041. https://doi.org/10.1088/1367-2630/11/7/073041
29. Hemme P, Li CH, Djemia P, et al (2021) Elastic and magnetoelastic properties of TbMnO3 single crystal by nanosecond time resolved acoustics and first-principles

calculations. Journal of Physics: Condensed Matter 33:495402. https://doi.org/10.1088/1361-648X/ac25ad

30. Zhou X, Gall D, Khare SV (2014) Mechanical properties and electronic structure of anti-ReO3 structured cubic nitrides, M3N, of d block transition metals M: An ab initio study. Journal of Alloys and Compounds 595:80–86. https://doi.org/10.1016/j.jallcom.2014.01.116

31. Yen C-Y, Jian S-R, Lai Y-S, et al (2010) Mechanical properties of the hexagonal HoMnO3 thin films by nanoindentation. Journal of Alloys and Compounds 508:523–527. https://doi.org/10.1016/j.jallcom.2010.08.109